ACS APPLIED ENERGY MATERIALS

www.acsaem.org
Article

Plasma-Assisted Synthesis in Aqueous Solution to Prepare Ir-Based Nanocatalysts for Oxygen Evolution Reaction in Acidic Conditions

Alexey Treshchalov, Heiki Erikson, Milutin Smiljanić,* Milena Šetka, Lazar Bijelić, Marjan Bele, Martin Šala, Siim Pikker, Peeter Ritslaid, Nejc Hodnik,* and Kaido Tammeveski*

Cite This: ACS Appl. Energy Mater. 2025, 8, 7084−7094

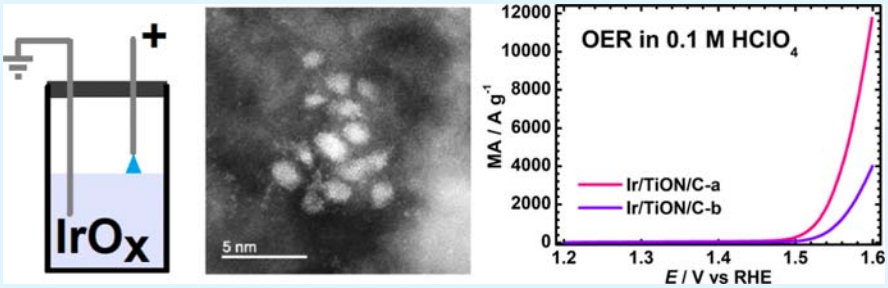

ABSTRACT: Green hydrogen production is a key factor in reaching climate goals. Proton exchange membrane water electrolysis (PEMWE) is one of the most promising technologies to achieve this, but it is limited by the poor electrocatalytic activity of the oxygen evolution reaction (OER), which requires high loadings of expensive and scarce precious metals, such as iridium. In this study, we synthesized iridium nanoparticles supported on titanium-oxynitride-decorated reduced graphene oxide (TiON/C). The prepared materials have been characterized using a variety of physicochemical methods, and the OER activity of iridium-based catalysts was assessed by cyclic voltammetry in acidic media. The plasma-assisted synthesis approach enables the preparation of electrocatalysts without the need for reducing agents, high-temperature annealing, or any other post-treatment. An outstanding mass-specific activity value of 11,700 A g^{-1} reached at 1.6 V_{RHE} was obtained for the prepared Ir/TiON/C catalyst. The small Ir particle size and strong Ir−TiON interactions contribute significantly to the enhanced OER activity and good stability, demonstrating the potential of this material for efficient and sustainable hydrogen production with PEMWE.

KEYWORDS: *oxygen evolution reaction, plasma-assisted synthesis, IrO_x nanoparticles, TiON support, water electrolysis, PEMWE*

1. INTRODUCTION

To reach climate goals, several countries have formulated their targets and the European Union has signed the European Green Deal.[1] Hydrogen plays a crucial role in reaching the set goals, which means that the level of production of H_2 must be increased. One approach to enhancing the production of green H_2 is to use electrolysis. Alkaline water electrolyzers can be considered as a mature technology; however, the need for a diaphragm to separate the anode and cathode decreases the efficiency and leads to safety issues.[2,3] Proton exchange membrane water electrolyzers (PEMWE) have higher productivity and are compact and more efficient, but they require precious metal catalysts and corrosion-resistant stack components.[4] The precious metals used in PEMWE are platinum, ruthenium, and iridium, and focus has been set to improve their utilization in those devices, particularly on the anode where the Ir-based catalysts are used to run the oxygen evolution reaction (OER).[5] The sustainable utilization of Ir, in particular, needs to be addressed due to its extreme scarcity in the Earth's crust, resulting in only below 10 tons of yearly production.[6]

Various structures can be prepared to increase the activity of the catalyst. For example, iridium dendrites comprising ca. 10 nm particles have been shown to possess higher OER currents than commercial Ir catalysts, which was attributed to an increased surface area.[7] It is agreed that different iridium species result in different OER activities. Stephens and co-workers suggested that optimal Ir-based catalysts for OER would possess an intrinsic reaction rate of IrO_2 and active site density of amorphous iridium oxide.[5] They came to that conclusion by theoretical calculations supported by experimental evaluation of ca. 100−200 nm amorphous IrO_x and larger rutile IrO_2 particles. Yu et al. reported that amorphous IrO_2 is needed for active OER catalysts particularly when

Received: February 13, 2025
Revised: May 13, 2025
Accepted: May 13, 2025
Published: May 17, 2025

https://doi.org/10.1021/acsaem.5c00444
ACS Appl. Energy Mater. 2025, 8, 7084−7094

prepared so that it has a high number of defects and low valence Ir.[8] Mixed-phase IrO_2 catalysts were evaluated toward OER and the recorded high activity was suggested to arise from the movement of oxygen species to the 1 T phase from the rutile phase.[9] The same effect was highlighted to improve the catalyst durability, as it inhibits the migration of oxidized Ir species at anode potentials. Ir−Ti mixed oxides could be a solution to reduce Ir content in active OER catalysts.[10]

However, the electrocatalytic activity of the catalyst is not the only factor that must be focused on; the stability of the materials must also be assessed. Cherevko et al. evaluated the activity and stability of metallic Ir as well as electrochemically grown hydrous iridium oxide for OER.[11,12] They summarized that the dissolution of Ir and its activity are parallel processes with common intermediate species. Thus, options to increase the stability of the Ir-based catalysts must be sought.[13] As previously discussed, there has to be a balance between the forms of Ir to have high OER activity and low dissolution of the metal. One way to combat the dissolution of Ir is to design supports to stabilize the catalyst, for example, through strong metal−support interactions.[13]

One could use platinum to decrease the Ir loading and improve catalyst stability,[14] but the price concerns would remain. Ledendecker et al. used tin oxide and coated those particles with Ir oxide by atomic layer deposition (ALD).[15] This approach decreases the amount of precious metals but introduces difficulties in the preparation of the catalyst due to different surface energies and temperature-induced mixing in the preparation of rutile IrO_2. They suggested that overcoming these difficulties could yield catalysts similar to the best Ir-based materials with improved stability.[15] Another good strategy is to use both doped and undoped TiO_2 as a support material for Ir oxides. Thus, Frisch et al. used templated ALD to prepare Ir- and IrO_x-coated mesoporous $IrTiO_x$ catalysts.[16] They reached above 2600 A g^{-1} at 1.6 V_{RHE} in a rotating disk electrode setup as a higher amount of Ir species was said to be accessible for the reactants as compared to conventional material. Böhm et al. investigated $IrOOH_x$-coated TiO_2 catalysts with different Ir contents and heat treatments.[17] They reported that such an Ir-based catalyst with 30 wt % Ir that was heat-treated at 375 °C surpassed the mass-activity of commercial Ir-based catalysts in a liquid cell up to 8 times.[17] Using thin-film $IrTiO_x$, it was shown that 300 °C is suitable to prepare the intermixed catalyst by varying the Ir-to-Ti ratios to tune the OER activity and stability.[18] Also, IrO_2/TiO_2 catalysts with a 4/2 ratio have shown to be the best for OER.[19] Bernicke et al. concluded that the Ir content in TiO_2 should be at least 30 wt % as otherwise, the electrical conductivity is not sufficient.[20] Also, 500 °C has been found to be suitable to prepare Ir shell-TiO_2 core particles as iridium is transferred to the surface by annealing under an H_2-containing atmosphere.[21] A simple approach to prepare an IrO_2/TiO_2 OER catalyst is to use UV photodeposition.[22] This approach enables the preparation of IrO_2 directly onto TiO_2 with small particle size and very good distribution to yield similar OER activity as unsupported IrO_2.[22,23] These research studies suggest that different catalyst preparation methods must be optimized separately, and one specific ratio or temperature treatment might not be optimal for all. For improved mass transport, the macroporosity is needed to enhance the OER activity.[24]

A good dopant to improve the OER electrocatalytic activity of IrO_2/TiO_2 is boron as it increases the electrical conductivity and contributes to the formation of the OER intermediates to boost the activity.[25] Nitrogen is also a good dopant, and it is used to create TiON to be utilized as a catalyst support. When using TiON alone as the OER catalyst, the oxidation of oxynitride should not be overlooked;[26] however the Ir on that support significantly changes the oxidation behavior of the TiON.[27] TiO_xN_y-supported Ir catalysts with low Ir content can have OER mass-activity around 450 A g^{-1} at 1.55 V_{RHE}.[28] In this case, the support consists of different Ti species like oxynitride, nitride, and oxide, which ensure good electrical conductivity that contributes to the OER activity and stability. Also, TiN may be considered as a support for OER catalysts as IrO_x/TiN has outperformed IrO_x supported on metallic Ti.[29] By careful design and synthesis, low amounts of Ir have been deposited onto defective TiN_{1+x} support so that the resulting catalyst exhibits more than 7 times higher mass-activity than that of IrO_2.[30] Zhang et al. prepared 1.4 nm IrO_2 nanoparticles onto TiN support that outperforms IrO_2, but the stability of this material was low, which was deemed to be due to the small particle size.[31] A method to prepare IrO_x nanoparticles through hydrolysis has been reported and in optimal conditions, the OER activity surpasses that of commercial IrO_2.[32]

As defect-free TiO_2 itself is an electrical insulator, in addition to doping, researchers have prepared various composites to improve the electrical conductivity of the catalyst. Carbon powder can be used as a support for Ir; however, the stability of the carbon in OER conditions is a major issue.[33] To overcome the stability issues, one could use carbon nanomaterials like carbon nanotubes (CNT) in combination with TiO_2, so the CNTs are protected from corrosion by overlaying a uniform TiO_2 layer.[34] Such a TiO_2/CNT composite has similar electrical conductivity as Vulcan carbon and when Ir was deposited onto this support, then higher activity and stability were recorded than that of analogous material without the TiO_2 layer. One of the reasons for enhanced activity was said to be that TiO_2 promotes the formation of Ir^{3+} species to boost the OER.[34] Strong synergistic effect has been reported for Ir supported on $TiON_x$ and reduced graphene oxide nanoribbon carbon-ceramic catalyst yielding mass activities that exceed 4800 A g^{-1} at 1.55 V_{RHE}.[6] A key factor for high OER activity was fine-tuning of the support (the ratio between graphene nanoribbons and $TiON_x$).

Plasma-liquid systems have attracted increasing attention in recent years, owing to their high potential in nanomaterial processing.[35,36] During the plasma-liquid treatment, reducing or oxidizing agents can be directly produced at the plasma-liquid or electrode-liquid nanointerfaces, which is a key advantage of this technique in contrast to the conventional wet-chemical methods.[35,36] Nonthermal atmospheric pressure plasma-assisted synthesis of nanoparticles (NP) in aqueous solutions is a one-step method with relative simplicity, fewer chemical reagents, high reaction yield, fast processing rates at room temperature, and the absence of side products. Most importantly, it is possible to avoid surfactants because the synthesized NPs are usually stabilized electrostatically.[37]

Previously we have used plasma-assisted synthesis to prepare Ag, Pd, and Pt nanoparticles for electrochemical application in the oxygen reduction reaction.[38−40] This approach enables the preparation of nanoparticles through simple, cost-effective processing and does not require further stabilizing agents. In this study, we employ this technique to prepare Ir oxide nanoparticles and subsequently deposit them onto the TiON/C support to evaluate their oxygen evolution reaction activity in 0.1 M $HClO_4$ solution. The physicochemical character-

https://doi.org/10.1021/acsaem.5c00444
ACS Appl. Energy Mater. 2025, 8, 7084−7094

Scheme 1. Preparation of Ir-Based Catalysts Using a Plasma-Assisted Approach

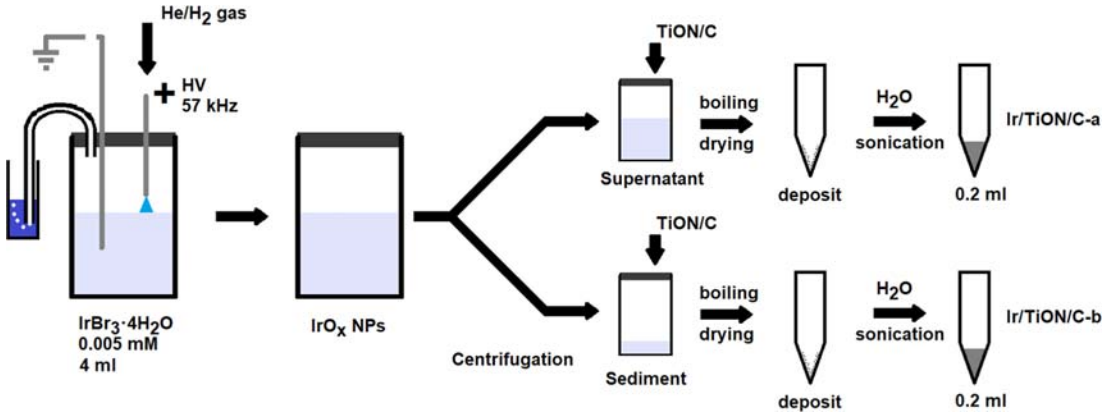

ization was carried out using scanning and transmission electron microscopies, X-ray photoelectron spectroscopy, and Raman spectroscopy, while the Ir content was determined using inductively coupled plasma mass-spectroscopy.

2. EXPERIMENTAL SECTION

2.1. Catalyst Synthesis. A simple, one-step plasma-assisted synthesis method similar to that described in our previous works[39,41] was applied for the preparation of IrO_x nanoparticles (NPs) in aqueous solutions. The catalyst preparation is summarized in Scheme 1. Briefly, an atmospheric pressure pulsed (57 kHz) unipolar discharge in a He/H_2 (95/5) gas jet with a continuous gas flow of 100 sccm was utilized in the plasma processing procedure. The purity of He and H_2 gases was 5.0 (Linde Gas). For the synthesis, 4 mL of 0.005 mM $IrBr_3{\cdot}4H_2O$ aqueous solution was used as an electrolyte in a sealed glass vessel. The current flow (the averaged value of about 40 mA) was arranged from a stainless-steel capillary (inner diameter of 150 μm) serving as the anode through a plasma jet and over the electrolyte to a grounded Pt foil counter electrode as a cathode (with the area of 0.5 cm^2) immersed in the liquid. The distance between the capillary tip and the liquid surface was about 5 mm. The pH of the start solution was 5.8 and it remained nearly unchanged after the plasma treatment. The temperature of the liquid did not exceed 50 °C during the plasma processing. High overpotential and pulsed current density as well as very short nucleation−growth time provide the ideal driving force for electrochemical deposition of small NPs at high density over the Pt foil surface. We noticed that after several synthesis experiments, a thin blue deposit of IrO_x NPs appeared on the surface of the Pt foil. To prevent the accumulation and agglomeration of IrO_x NPs, a very diluted solution of the $IrBr_3{\cdot}4H_2O$ salt was used as an electrolyte. During the plasma processing, sonication of the solution was arranged by a low-power (~1 W) ultrasonic (1.7 MHz) transducer that contacted the bottom of the glass vessel. The principal role of ultrasound is the increase in mass transfer induced by extreme solution mixing caused by cavitation microjets.[42] These jets initiate effective cleaning of the electrode surface from the created IrO_x NPs.

The solution was deaerated by bubbling helium gas with a flow rate of 100 sccm for 10 min before plasma ignition. Pulsed He/H_2 plasma has the advantage compared with pure He or Ar plasma: the lack of NO_x (the absence of additional acidification of the solution) and OH^*_{aq} species (the absence of hydrogen peroxide production in the solution). After 15 min of plasma treatment, the colloidal solution of IrO_x NPs was centrifuged (15 min at 12,000g) to separate small NPs from relatively big agglomerates. These two fractions (supernatant and sediment) were tested separately.

The first one (supernatant with small NPs) was dispersed by sonication with 0.1 mL of aqueous dispersion of TiON/C support (the concentration of support suspension is 8 mg mL^{-1}). After that, water was evaporated by boiling at 100 °C. The dry deposit was dispersed by sonication with 0.2 mL of water in the test tube, and this colloidal solution was the final catalyst product. This material is designated as Ir/TiON/C-a.

The second fraction (0.2 mL of sediment after centrifugation with relatively large IrO_x NPs) was dispersed by sonication with 0.1 mL aqueous suspension of 8 mg mL^{-1} TiON/C support. After drying at 60 °C, 0.2 mL of water was added to the dry deposit in the test tube, and after sonication, this colloidal solution was the final catalyst product. This material is designated as Ir/TiON/C-b.

The drying procedure was employed to facilitate a more homogeneous dispersion of IrO_x NPs onto the TiON/C support. We assume that during the drying step, the IrO_x nanoparticles are attached to the support and do not come off from the TiON/C surface with further processing.

2.2. Physicochemical Characterization of the Catalysts. Prepared materials were characterized using Thermo Scientific Apreo 2 (Thermo Fisher Scientific Inc., UK) field emission SEM, equipped with an EDS spectrometer − silicon drift detector EDX UltimMax 100 (Oxford Instruments, Oxford, UK). The operational voltage was set to 7 kV for the SEM measurements. Additional imaging and characterization were performed on an FEI Nova Nanosem 450 FE-SEM (Thermo Fisher Scientific Inc., UK) at 5 kV, spot size of 3, and by using a through-lens detector (TLD). Ir/TiON−C samples were also characterized using scanning transmission electron microscopy (STEM) imaging (JEOL JEM-ARM200CF Ltd., Tokyo, Japan) operated at 80 kV. For this purpose, TEM grids were coated with 5 μL of the catalyst ink and allowed to dry in a clean environment.

X-ray photoelectron spectroscopy (XPS) analyses were performed using a Versa probe 3 AD (Phi, Chanhassen, USA) instrument equipped with a monochromatic Al Kα X-ray source operating at an accelerating voltage of 15 kV and an emission current of 13.3 mA. The samples were drop-coated on the silicon wafer, dried, and analyzed in an ultrahigh vacuum environment, with a base pressure of approximately 10^{-9} Torr. Survey scans were acquired with a pass energy of 224 eV and a energy step of 0.8 eV. The energy resolution was set to 0.1 eV and the pass energy for high-resolution spectra was 27 eV. Charge neutralization was applied to compensate for any surface charging during analysis, and all binding energies were calibrated to the C 1s peak at 284.4 eV as a reference. Data were processed and analyzed using CasaXPS Version 2.3.26 software.

Micro-Raman spectra were recorded in the backscattering geometry on an inVia Renishaw spectrometer in conjunction with a confocal microscope (Leica Microsystems CMS GmbH), 50× objective, and an argon ion laser operated at 514.5 nm. Samples of the catalyst ink were drop-coated on silicon substrates and dried at room temperature. Low incident laser intensity at the sample was used to prevent excessive sample heating and/or decomposition.

A Jasco V-570 UV/vis/NIR spectrophotometer with 1 cm silica cell was used to measure the optical absorption spectra of various solutions to evaluate the progress of the synthesis.

https://doi.org/10.1021/acsaem.5c00444
ACS Appl. Energy Mater. 2025, 8, 7084−7094

2.3. Electrochemical Characterization of the Catalysts. Glassy carbon disks (GC, d = 5 mm, GC-20SS, Tokai Carbon) embedded into Teflon holders were cleaned prior to each experiment with 1200 grit emery paper and polished to a mirror finish using alumina slurries (1 and 0.3 μm, Buehler). The polishing residues were removed by ultrasonic treatment in water and 2-propanol (Fisher Scientific). In a typical experiment, 20 μL of catalyst ink (see catalyst preparation section) was drop-cast onto freshly cleaned GC electrodes and was allowed to dry at 60 °C after which 5 μL of Nafion solution (5 wt % in lower aliphatic alcohols, Ion Power Inc., diluted 1:50 in 2-propanol) was drop-cast onto the catalyst-coated GC electrode.

The oxygen evolution reaction activity was assessed in 0.1 M $HClO_4$ solution made using Milli-Q water and 70% $HClO_4$ (99.999% trace metal basis, Sigma-Aldrich). The electrochemical measurements were conducted using Autolab potentiostat/galvanostat PGSTAT128N in a three-electrode configuration where Pt wire separated by glass frit and reversible hydrogen electrode (RHE) connected with Luggin capillary served as counter and reference electrodes, respectively. Prior to the OER measurements, the electrodes were conditioned by scanning 50 potential cycles from 1.2 to 0.05 V at 200 mV s^{-1} and 50 cycles in the potential range of 1.2−1.6 V at 100 mV s^{-1} and the OER was measured in the potential range of 1.2−1.6 V at 5 mV s^{-1}. Stability tests were carried out by applying potential with a square wave, that is, 1.6 V was applied for 3 s followed by 3 s at 0.05 V for a total of 1500 pulses and after every 100th cycle, OER polarization curve (1.2 to 1.6 V at 200 mV s^{-1}) and CV (1.2 to 0.05 V at 5 mV s^{-1}) were recorded. The working electrode was set to rotate at 3500 rpm during the stability measurements to remove the formed oxygen bubbles.

3. RESULTS AND DISCUSSION

3.1. Characterization of Ir/TiON/C-a and Ir/TiON/C-b Catalysts. Figure S1 shows the UV extinction spectra of the starting and plasma-treated solutions. The spectra were corrected to pure water absorption and scattering, as well as cell window reflectivity losses. After the plasma processing, the initial spectrum (red curve) transforms to the spectrum of colloidal solution, where both larger and smaller IrO_x NPs are present (black curve). The tail at ∼220−400 nm belongs to the Rayleigh scattering of Ir-IrO_x NPs.[43] The ∼195 nm band belongs to the presence of Br^- ions, which are produced from $IrBr_3$ species during the plasma processing. For comparison, the spectrum of 0.014 mM NaBr is added to the graph (green curve). The spectrum of the supernatant after centrifugation of the plasma-treated solution (blue curve) shows a decrease of the scattering tail due to removing of relatively big IrO_x NPs; however, some scattering from small IrO_x NPs is still visible in the spectrum. These data confirm that during the synthesis, two fractions of IrO_x NPs are produced.

During plasma processing, a high local alkalization is generated near the cathodic Pt foil due to the electrochemical decomposition of water: $2H_2O + 2e^- \rightarrow H_2 + 2OH^-$. At the same time, strong local acidification takes place in the plasma-liquid interface layer, which is caused by intensive bombardment by ions from plasma. We may speculate that due to the hydrolysis of $IrBr_3$ species, $[Ir(OH)_6]^{3-}$ or $[Ir(H_2O)_6]^{3+}$ complexes are formed and possibly undergo a polycondensation process on the Pt foil surface. Due to the low initial concentration of $IrBr_3$ species, their transport-limited depletion layer near the cathode interface is produced. Therefore, the size of the synthesized IrO_x NPs is inherently limited by the amount of reactants in the depletion layer. Besides, the growth of IrO_x NPs is stopped by the electrostatic stabilization mechanism until a sufficient negative surface charge on the IrO_x NPs is accumulated by OH^- adsorption in a strongly alkaline interface layer. If the plasma-assisted synthesis is arranged with higher concentrated $IrBr_3$ solutions (0.25−0.05 mM) or in acidic conditions (pH < 4), mainly big (∼2 μm) flat Ir or IrO_x flakes composed of sticking together NPs are produced (see Figure S2 in the Supporting Information). In acidic conditions, the hydrogen evolution reaction occurs on the cathode ($2H_3O^+ + 2e^- \rightarrow H_2 + 2H_2O$), so the electrostatic stabilization mechanism is absent without the production of OH^- ions.

Raman spectra of Ir/TiON/C-b catalysts are shown in Figure 1. Broad Raman bands at 480 and 611 cm^{-1} belong to

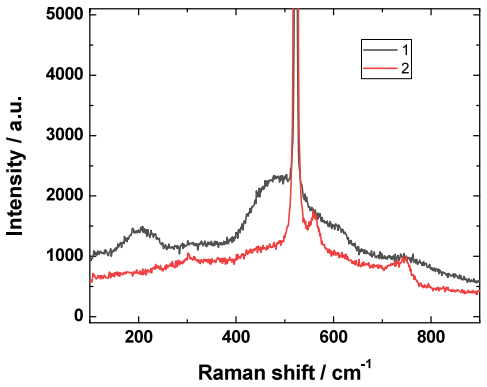

Figure 1. Raman spectra of the Ir/TiON/C-b catalyst: Spectrum 1 was measured with a low-intensity laser and spectrum 2 was measured after the local heating of the sample with a high-intensity laser.

IrOx species with poor crystallinity. Narrow peaks at 561 and 747 cm^{-1} belong to typical Ir−O vibrations of rutile IrO_2 species with a higher crystallinity. The strong line at 520 cm^{-1} is from the Si substrate. Spectrum 2 shows that after the local annealing by intense laser irradiation, amorphous IrO_x transforms to rutile IrO_2 species with higher crystallinity.[44]

Ir nanocatalysts supported on a TiON/C composite prepared by the plasma-assisted synthesis method are characterized by SEM as shown in Figure 2. The SEM

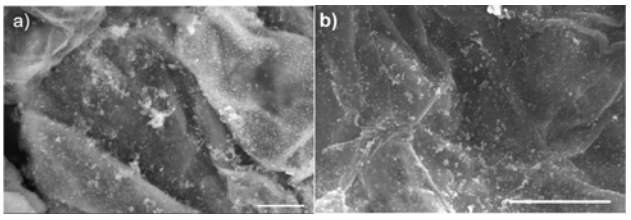

Figure 2. SEM imaging of (a) Ir/TiON/C-a and (b) Ir/TiON/C-b samples. Scale bars: 1 μm.

imaging of the Ir/TiON/C-a and Ir/TiON/C-b samples, Figure 2a,b, reveals that the graphene oxide nanoribbons are decorated by TiON flakes. In Figure 2a Ir nanoparticles cannot be easily discerned using SEM at these magnifications due to the low loading and small size. However, in Figure 2b, bigger Ir nanoparticles can be noticed.

To get a closer look at the formed Ir nanoparticles, we performed STEM imaging. The STEM image together with EDX mapping of the Ir/TiON/C-a sample is presented in Figure 3. STEM image shows an Ir nanoagglomerate, which appears to be composed of numerous smaller clusters that together form a very porous sponge-like nanostructure. Such

https://doi.org/10.1021/acsaem.5c00444
ACS Appl. Energy Mater. 2025, 8, 7084−7094

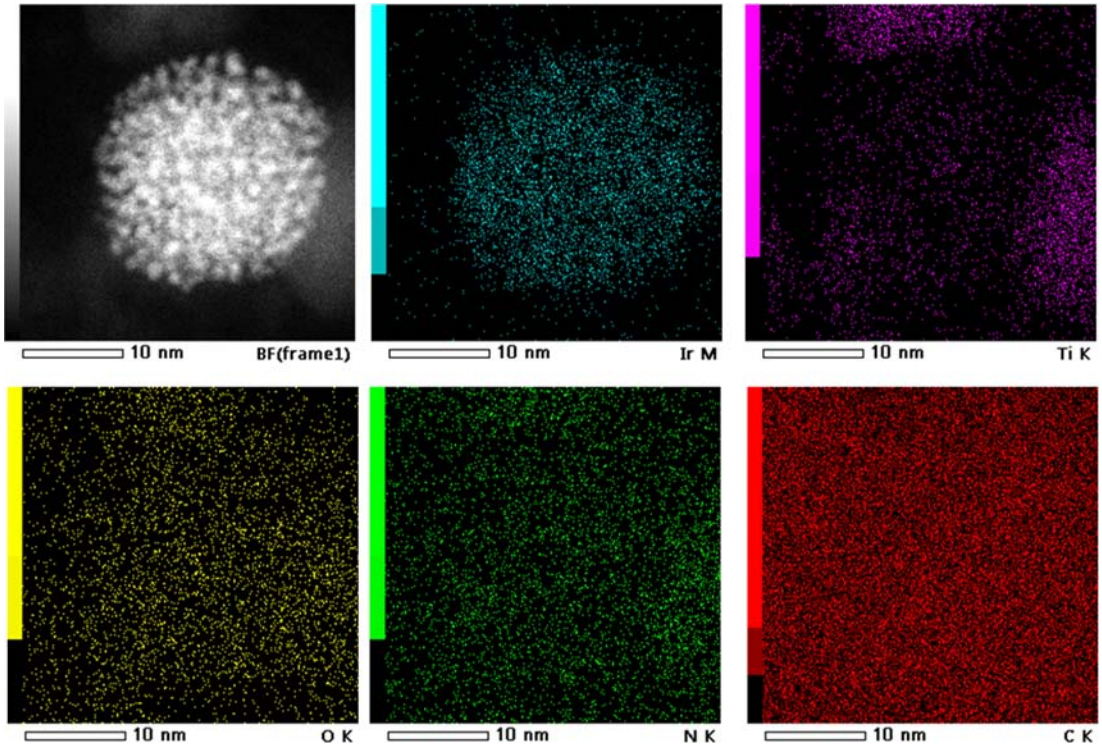

Figure 3. STEM imaging of the Ir/TiON/C-a sample (representative single Ir nanoagglomerate with sponge-like morphology) coupled with EDX mapping.

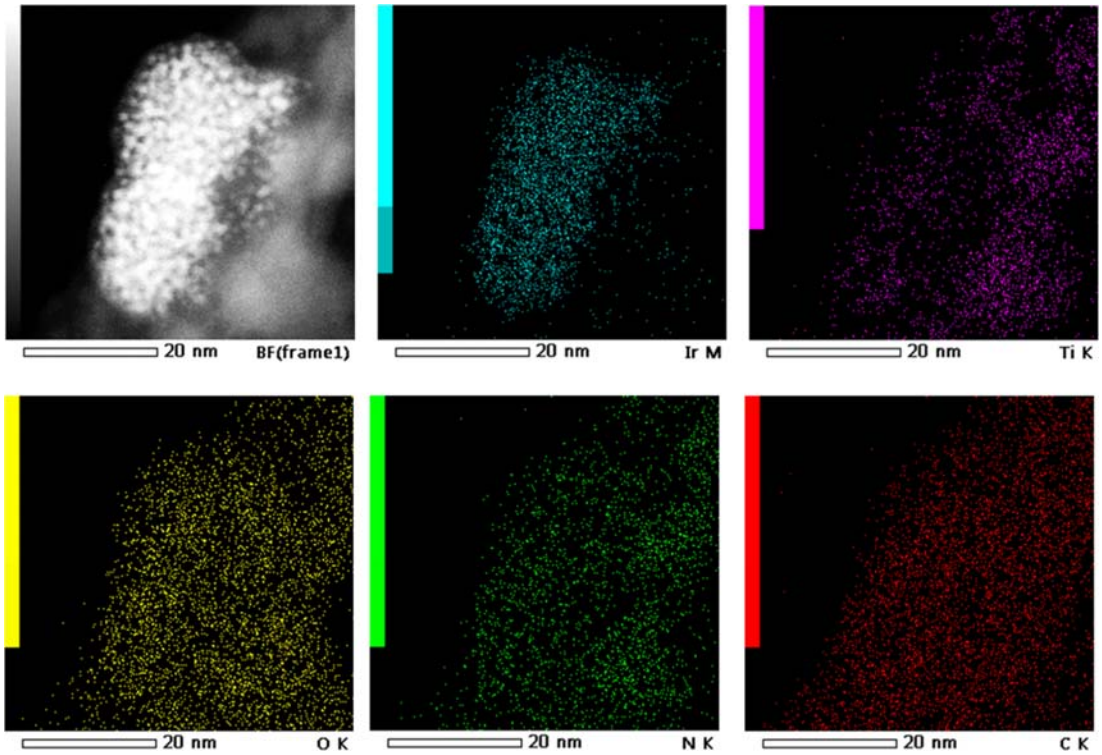

Figure 4. STEM imaging of the Ir/TiON/C-b sample coupled with EDX mapping.

nanostructures feature a particularly high specific surface area, making them very attractive for electrocatalytic purposes. EDX elemental mapping confirms that the Ir nanoparticle is attached to the TiON flake, providing the necessary platform for the metal–support interaction.

STEM imaging of the Ir/TiON/C-b sample is given in Figure 4. Similarly, Ir nanostructures with sponge-like morphology are obtained by the applied synthesis approach. EDX mapping confirms the presence of Ir nanoagglomerate which is in contact with TiON.

https://doi.org/10.1021/acsaem.5c00444
ACS Appl. Energy Mater. 2025, 8, 7084−7094

Interestingly, we noted that Ir nanoagglomerates display strong beam sensitivity manifested through a coarsening effect that leads to the formation of larger Ir crystallites/domains within the nanoagglomerates, as depicted in Figure S3. In cases where there is a thick amorphous IrO_X shell, exposure to the beam seems to result in crystallization, Figure S4. It is likely that reduction occurs in parallel to this process, where the valence state of Ir in IrO_X is reduced; however, an analysis of the oxidation state using electron energy-loss spectroscopy (EELS) was thus impractical to perform precisely because of beam-induced reduction. Still, we believe we could take an image of the state of the Ir catalyst before it coarsened.

Sample Ir/TiON/C-a contains only a minor fraction of beam-sensitive amorphous nanoagglomerates of IrO_X, which are mostly presented in the Ir/TiON/C-b sample. In this case, Ir particles of ∼1−3 nm are present (Figure 5a), in addition to a large number of Ir single atoms and atom clusters distributed over TiON flakes (Figure 5b). Longer exposures of the sample to the electron beam did not seem to lead to changes in either particles or atomic clusters.

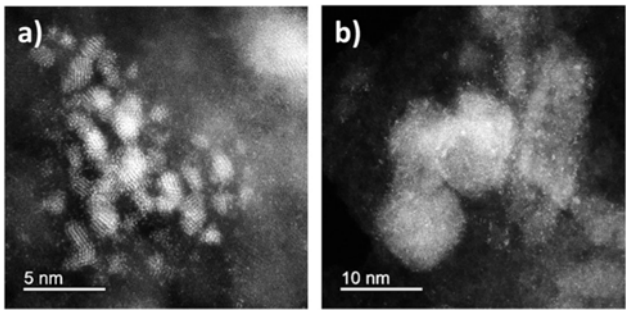

Figure 5. High-angle annular dark-field STEM images of sample Ir/TiON/C-a showing (a) Ir nanoparticles and (b) Ir single atoms and clusters dispersed over the TiON/C support. Ir single atoms can be distinguished from TiON/C as bright spots, owing to their higher atomic number.

Figure 6 reports the XPS spectra of the Ir/TiON/C-a and Ir/TiON/C-b samples, showing characteristic peaks for carbon (C 1s), nitrogen (N 1s), titanium (Ti 2p), and oxygen (O 1s). Both samples display similar intensities for C 1s, N 1s, and O 1s, while Ti 2p demonstrates a higher surface concentration in Ir/TiON/C-b. Sodium (Na 1s) was detected in both samples with a low signal intensity; however, the Ir/TiON/C-b sample exhibited a slightly higher Na 1s peak. Silicon peaks (Si 2p and Si 2s), originating from the Si wafer substrate used for sample deposition, are also visible in the spectra. Accurately identifying and quantifying the iridium (Ir 4f) peaks within wide XPS spectra is challenging due to their low loading in the sample and the overlap with Na 2s and Ti 3s peaks in the same binding energy region. Consequently, high-resolution spectra and detailed peak deconvolution were employed to reliably distinguish the individual contributions. The spectra of the Ir 4f region (57−68 eV) for the Ir/TiON/C-a (Figure 7a) and Ir/TiON/C-b (Figure 7b) samples reveal two characteristic bands at 62.0 eV (Ir $4f_{7/2}$) and 64.9 eV (Ir $4f_{5/2}$), confirming the predominant presence of Ir in the 4^+ oxidation state (e.g., IrO_2). Additionally, a partial contribution from Ir in the 3^+ oxidation state is observed as peaks at 62.9 eV (Ir $4f_{7/2}$) and 65.8 eV (Ir $4f_{5/2}$). The observed doublet peaks exhibit broader features compared to those reported in the literature for IrO_2 peaks,[44,45] primarily due to the overlapping contribution of Ti 3s and Na 2s peaks in the same binding energy region. Notably, the Ir 4f peaks in the Ir/TiON/C-b sample are broader compared to those in Ir/TiON/C-a, which is attributed to the higher concentration of Ti and Na species in the former sample. The XPS spectra in the Ti 3s region were fitted with three peaks at 61.3, 59.8, and 58.5 eV in both samples, which are assigned to Ti^{4+}, Ti^{3+}, and Ti^{2+} oxidation states, corresponding to TiO_2, Ti−O−N, and TiN species, respectively.[46,47] Fitting and the assignment of chemical states were guided by the initial analysis of the Ti 2p region as it is the most intense and well-defined for the XPS spectra of titanium. In the Ti 2p spectra (see Figure S5), we observed peaks at 458.1 eV (Ti^{4+}), 456.5 eV (Ti^{3+}), and 455.2 eV (Ti^{2+}), which are consistent with reported literature values.[45] Furthermore, the peak corresponding to Na 2s was included in the fitting for the Ir/TiON/C-b sample.

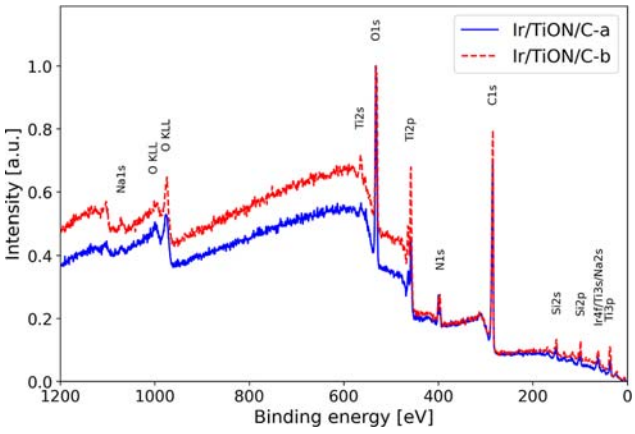

Figure 6. XPS survey spectra of Ir/TiON/C-a and Ir/TiON/C-b samples.

3.2. OER Studies. First, the CVs of the prepared catalyst materials were recorded in 0.1 M $HClO_4$ solution for their pretreatment and electrochemical characterization (Figure 8a). The CVs of both of the materials show typical behavior of oxidized Ir as they both have a pair of broad maxima at ca. 0.95 V as well as at 0.55 V and no peaks associated with hydrogen adsorption/desorption.[7,48] Ir/TiON/C-a exhibits slightly more pronounced pair of peaks at 0.55 V. The CV peak at 0.95 V originates from Ir(III)/Ir(IV) redox reaction and the prepeak at ca. 0.55 V could be due to the oxidation of Ir(III) near the metal/oxide interface.[17] This suggests that the interaction between Ir and TiO_2 is stronger immediately after the electrochemical pretreatment of the material given that the Ir particles are smaller. Lee et al. discussed that the oxidation degree of the surface affects the CV response and also the OER activity.[7]

The initial OER activity was assessed with the prepared materials, and the OER polarization curves are presented in Figure 8b. The mass-activities for the OER were calculated by normalizing the measured current with respect to the mass of Ir determined from the ICP−MS measurements where it was found that the Ir contents of Ir/TiON/C-a and Ir/TiON/C-b were 2.83 and 7.78 mg kg^{-1}, respectively. This means that the Ir content in the catalysts is extremely low in both cases. From Figure 8b, it is obvious that Ir/TiON/C-a has better onset potential and significantly higher MA. This could be due to the better interaction between Ir and TiON of the former, as the

https://doi.org/10.1021/acsaem.5c00444
ACS Appl. Energy Mater. 2025, 8, 7084−7094

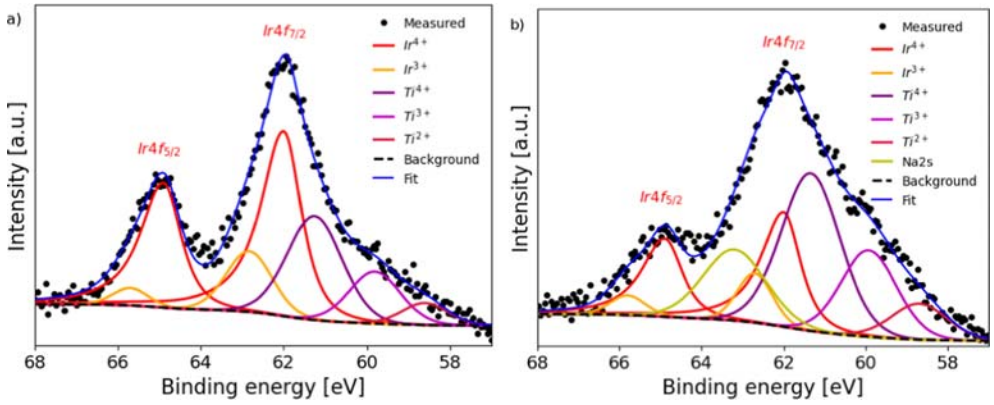

Figure 7. High-resolution XPS spectra of the Ir 4f region for Ir/TiON/C-a (a) and Ir/TiON/C-b (b) samples.

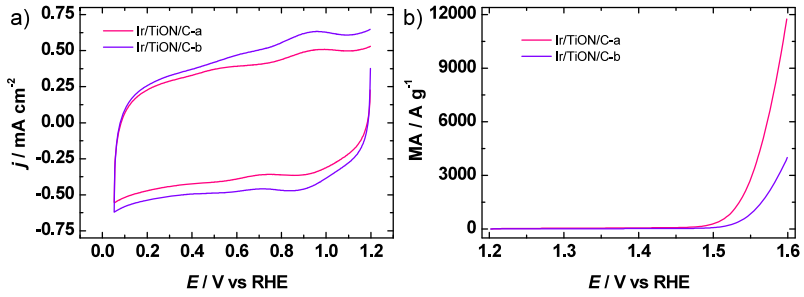

Figure 8. (a) 50th CV of the pretreatment of Ir/TiON/C catalysts, ν = 200 mV s^{-1}. (b) OER polarization curves, ν = 5 mV s^{-1}. Solution: 0.1 M $HClO_4$.

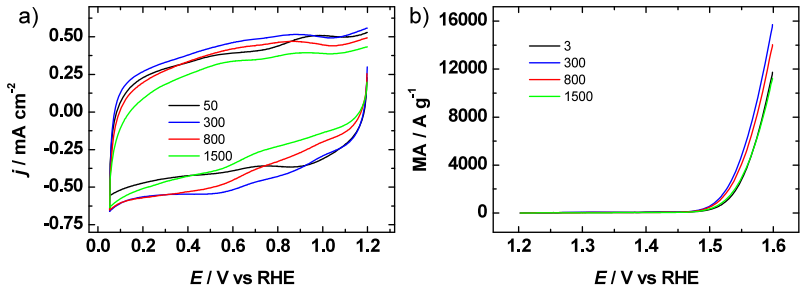

Figure 9. (a) Evolution of the CVs of Ir/TiON/C-a during the OER stability testing, ν = 200 mV s^{-1}. (b) Evolution of OER mass activity during the stability testing, ν = 5 mV s^{-1}. Solution: 0.1 M $HClO_4$.

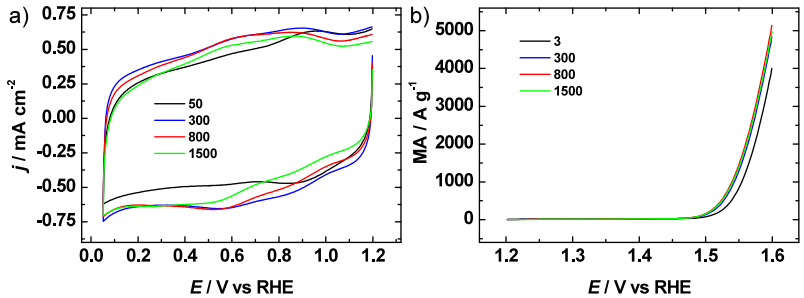

Figure 10. (a) Evolution of the CVs of Ir/TiON/C-b during the OER stability testing, ν = 200 mV s^{-1}. (b) Evolution of OER mass activity during the stability testing, ν = 5 mV s^{-1}. Solution: 0.1 M $HClO_4$.

CV hinted. Tafel analysis revealed a slope of 50 mV for both materials (Figure S5), which is typical for a variety of Ir-based OER catalysts (Table S1).

Stability testing was carried out to assess the catalyst materials further. Sample Ir/TiON/C-a showed that the OER current at 1.6 V increases for the first 300 potential cycles of stability testing, and then it starts to decline reaching the initial value after around 1400 start−stop cycles (Figure 9). The electrode response changes significantly during the first 100 potential pulses as a broad ill-defined prepeak at about 0.55 V

https://doi.org/10.1021/acsaem.5c00444
ACS Appl. Energy Mater. 2025, 8, 7084−7094

is observed in the CV (Figure 9a). This could be attributed to reorganization of the surface and its cleaning. The change in the prepeak could be associated with the improved interaction between Ir and support.[17] The peak at 0.95 V starts to decrease with further potential pulses, and after ca. 300 pulses, the CV is at a steady state and further changes could be attributed to the loss of active material and Ostwald ripening. With the surface reorganization of the catalyst, the OER mass activity improves rapidly and then starts to decline. Thus, at least 300 potential pulses are needed to obtain the highest OER activity as a result of improved interaction between iridium and TiON. The form of iridium is also important in addition to the interaction between iridium and support.[16] Zhang et al. proposed that high-valence IrO_x forms on the surface of the IrO_x/TiO_2 in the OER conditions and that it is the core reason for the high activity of the catalyst.[49] This could explain the observed change in CV behavior.

Sample Ir/TiON/C-b showed similar tendencies that the broad preoxidation peak formed during the stability testing and after 500 cycles the CV was at steady state (Figure 10). Further changes in the CV could be attributed to the loss of the catalyst material. In terms of the OER activity, an improvement was observed until 800 on−off cycles after which the electrocatalytic activity started to decline, but the decline was not as severe as in the case of Ir/TiON/C-a.

The initial MA value at 1.6 V_{RHE} for Ir/TiON/C-a reached 11,700 A g^{-1}, while that for Ir/TiON/C-b reached 4000 A g^{-1}. This shows that small IrO_x NPs are ∼3 times more active than large agglomerated NPs. During the stability testing, the MA improves to impressive 15,700 and 5100 A g^{-1} for Ir/TiON/C-a and Ir/TiON/C-b catalysts, respectively. However, after 1500 potential cycles, the MA of Ir/TiON/C-a has dropped to a lower than the initial MA value of ∼11,000 A g^{-1} while Ir/TiON/C-b retains 5000 A g^{-1}. This behavior suggests that iridium in the Ir/TiON/C-a forms stronger interaction with the supporting TiON/C that enhances the OER activity, but the activity is decreasing due to the dissolution of Ir[11,12] or due to the formation of less active mixed oxides.[15] This is in line with the observations by Banti et al., who suggested that the interactions between Ir and TiO_2 enhance the mass-activity of such catalysts. The MA values obtained in the present study surpass those obtained with Ir single atom and cluster-based thin-film composites with TiON,[28] suggesting high utilization of Ir in this study. Similarly high OER MA values were obtained by Ohno et al. with Ir supported on Nb−SnO_2 and Ta−SnO_2.[50]

The better stability of Ir/TiON/C-b could be attributed to the bigger particle size but also to the agglomeration or simply due to the higher amount of iridium on the electrode. An important factor is also strong metal−support interaction (SMSI) that can significantly affect both the activity and stability of the material.[51] In our previous work, SMSI between TiON support and Ir active sites was described in detail using DFT calculations.[45] Briefly, it was shown that TiON can anchor Ir particles quite effectively, with N species being the preferred docking sites. Such behavior inhibits the sintering of Ir nanoparticles, which is beneficial for maintaining a high density of the active sites and thus high metal utilization. At the same time, electron charge redistribution occurs between Ir and TiON, which is the most pronounced at the Ir/TiON interface and diminishes with the increase in particle size. Therefore, in the tested samples, the described SMSI features can be expected since deposited Ir nanostructures include small particles, clusters, and even single atoms. Since these single atoms and clusters are mostly found in the Ir/TiON/C-a sample, a stronger SMSI can be expected than for the Ir/TiON/C-b composite. One must pay attention to the chosen stability testing protocol as it could affect the result as has been reasoned previously.[51] Despite having multiple protocols for stability measurements, the start−stop approach used here gives a good initial assessment of the material behavior. The two materials prepared in this study show that plasma-assisted synthesis is a good method to prepare active and stable Ir/TiON/C catalyst for OER given that the synthesis protocol and Ir to support ratio are to be further optimized to maximize the SMSI. Van der Merwe et al. studied a series of Ir on TiO_x by varying the metal ratios and suggested that not only the Ir to Ti ratio is important but also the forms in which the metals are crucial factors.[18]

Another factor that affects the stability is the support material, particularly the nanocarbon used, as it corrodes at the OER potentials. We can assume that if the carbon support is not fully covered by either TiON or IrO_x then the carbon corrosion is faster, which means that the activity of the material drops earlier. Carbon support is used in the OER catalyst development thanks to its good electrical conductivity, but due to the instability at high potentials it must be protected, which can be done by covering it for example with TiO_2 or TiON and higher IrO_x content helps as well. There are studies in which TiO_2 and TiON have been coated onto different carbon materials like carbon nanotubes or reduced graphene oxide nanoribbons (rGONR) to be used as support for Ir nanoparticles as efficient and stable OER catalysts.[34,51] Moriau et al. varied the amount of TiON on rGONR and found that Ir nanoparticles on the edges of TiON are active OER catalysts as such composites benefit from the contact between Ir, TiON, and carbon.[51]

Finally, a couple of nonintrinsic factors that could influence the stability assessment of the OER should be mentioned. The formation of microscopic bubbles during gas-evolving reactions, such as OER, is shown to largely interfere with stability measurements, especially when working with thin films.[52] Even at high rotation rates, these bubbles could stick to the active sites and physically block them, producing a similar effect as degradation (i.e., activity decay). Another option for apparent activity decay can be found in the passivation of backing glassy carbon electrodes at OER conditions.[53] Although applied degradation tests were not particularly aggressive or long, it could be possible that the deactivation of the underlying glassy carbon led to the decay of the OER activity, which is not related to the degradation of Ir.

The results reported in this study demonstrate that plasma-assisted synthesis can be utilized to prepare highly active Ir-based electrocatalysts for the OER. Work to further optimize the synthesis procedure is in progress.

4. CONCLUSIONS

IrO_x nanoparticles were prepared by plasma-assisted synthesis and supported onto a TiON-decorated reduced graphene oxide. STEM analysis revealed that the formed nanoparticles form porous structures that would be beneficial for electrochemical reactions. ICP−MS analysis revealed a very low Ir loading in the catalyst, and due to the interactions between Ir and TiON, very high OER mass-activities of 11,700 A g^{-1} were obtained at 1.6 V_{RHE}. These results show that plasma-assisted synthesis is a very good and feasible approach to preparing

https://doi.org/10.1021/acsaem.5c00444
ACS Appl. Energy Mater. 2025, 8, 7084−7094

catalysts with high activity without needing complex and time and energy-consuming postprocessing or heat treatment.

■ ASSOCIATED CONTENT

Supporting Information

The Supporting Information is available free of charge at https://pubs.acs.org/doi/10.1021/acsaem.5c00444.

UV−vis spectra of prepared IrNPs, IrO_x nanostructures prepared in acidic conditions, STEM images of Ir nanoagglomerates displaying beam sensitivity, high-resolution XPS spectra in the Ti 2p region for Ir/TiON/C-a and Ir/TiON/C-b samples, Tafel plots, and comparison of kinetic parameters of various Ir-based OER catalysts (PDF)

■ AUTHOR INFORMATION

Corresponding Authors

Milutin Smiljanić − *Department of Materials Chemistry, National Institute of Chemistry, Ljubljana 1000, Slovenia;* orcid.org/0000-0002-4911-5349; Email: milutin.smiljanic@ki.si

Nejc Hodnik − *Department of Materials Chemistry, National Institute of Chemistry, Ljubljana 1000, Slovenia; Institute of Metals and Technology, Ljubljana 1000, Slovenia;* orcid.org/0000-0002-7113-9769; Email: nejc.hodnik@ki.si

Kaido Tammeveski − *Institute of Chemistry, University of Tartu, Tartu 50411, Estonia;* orcid.org/0000-0002-4144-4471; Email: kaido.tammeveski@ut.ee

Authors

Alexey Treshchalov − *Institute of Physics, University of Tartu, Tartu 50411, Estonia*

Heiki Erikson − *Institute of Chemistry, University of Tartu, Tartu 50411, Estonia*

Milena Šetka − *Department of Materials Chemistry, National Institute of Chemistry, Ljubljana 1000, Slovenia; Department of Chemical Engineering, University of Chemistry and Technology Prague, Prague 166 28, Czech Republic*

Lazar Bijelić − *Department of Materials Chemistry, National Institute of Chemistry, Ljubljana 1000, Slovenia;* orcid.org/0009-0007-7474-3236

Marjan Bele − *Department of Materials Chemistry, National Institute of Chemistry, Ljubljana 1000, Slovenia*

Martin Šala − *Department of Materials Chemistry, National Institute of Chemistry, Ljubljana 1000, Slovenia;* orcid.org/0000-0001-7845-860X

Siim Pikker − *Institute of Physics, University of Tartu, Tartu 50411, Estonia*

Peeter Ritslaid − *Institute of Physics, University of Tartu, Tartu 50411, Estonia;* orcid.org/0000-0002-3603-2237

Complete contact information is available at: https://pubs.acs.org/10.1021/acsaem.5c00444

Author Contributions

Conceptualization−A.T., M.S., N.H., K.T.; data curation−A.T., H.E., M.S.; formal analysis−A.T., H.E., M.S., M.Š., L.B., M.B., M.Š., S.P., P.R.; funding acquisition−S.P., N.H., K.T.; investigation−A.T., H.E., M.S., M.Š., L.B., M.B., M.Š., S.P., P.R.; methodology−A.T., H.E., M.S.; resources−A.T., M.S., N.H., K.T.; supervision−M.S., N.H., K.T.; validation−A.T., H.E., M.S.; visualization−A.T., H.E., M.S.; writing−original draft−A.T., H.E., M.S.; writing−review and editing−A.T., H.E., M.S., M.Š., L.B., M.B., M.Š. S.P., P.R., N.H., K.T.

Notes

The authors declare no competing financial interest.

■ ACKNOWLEDGMENTS

This work was supported by the Slovenian Research Agency through the funding of research program P2-0393 and I0-0003 and projects J2-50055, J7-50227, J2-50076, N2-0155, N2-0248, N2-0385, and NATO Science for Peace and Security Program under Grant G6230 and the Johannes Amos Comenius Programme, European Structural, and Investment Funds, project 'CHEMFELLS V' (No. CZ.02.01.01/00/22_010/0003004). The present work was financially supported by the Estonian Research Council (grant PRG2569). This research was also supported by the Estonian Ministry of Education and Research (TK210, Centre of Excellence in Sustainable Green Hydrogen and Energy Technologies) and was partially conducted using the NAMUR + core facility, which is funded by the projects "Center of Nanomaterials Technologies and Research" (2014-2020.4.01.16-0123) and TT13.

■ REFERENCES

(1) Pietzcker, R. C.; Osorio, S.; Rodrigues, R. Tightening EU ETS targets in line with the European Green Deal: Impacts on the decarbonization of the EU power sector. *Appl. Energy* **2021**, *293*, 116914.

(2) Brauns, J.; Turek, T. Alkaline Water Electrolysis Powered by Renewable Energy: A Review. *Processes* **2020**, *8* (2), 248.

(3) Miller, H. A.; Bouzek, K.; Hnat, J.; Loos, S.; Bernäcker, C. I.; Weißgärber, T.; Röntzsch, L.; Meier-Haack, J. Green hydrogen from anion exchange membrane water electrolysis: a review of recent developments in critical materials and operating conditions. *Sustain. Energy Fuels* **2020**, *4* (5), 2114−2133.

(4) Hughes, J. P.; Clipsham, J.; Chavushoglu, H.; Rowley-Neale, S. J.; Banks, C. E. Polymer electrolyte electrolysis: A review of the activity and stability of non-precious metal hydrogen evolution reaction and oxygen evolution reaction catalysts. *Renew. Sustain. Energy Rev.* **2021**, *139*, 110709.

(5) Liang, C.; Rao, R. R.; Svane, K. L.; Hadden, J. H. L.; Moss, B.; Scott, S. B.; Sachs, M.; Murawski, J.; Frandsen, A. M.; Riley, D. J.; Ryan, M. P.; Rossmeisl, J.; Durrant, J. R.; Stephens, I. E. L. Unravelling the effects of active site density and energetics on the water oxidation activity of iridium oxides. *Nat. Catal.* **2024**, *7* (7), 763−775.

(6) Moriau, L.; Smiljanić, M.; Lončar, A.; Hodnik, N. Supported Iridium-based Oxygen Evolution Reaction Electrocatalysts - Recent Developments. *ChemCatChem* **2022**, *14* (20), No. e202200586.

(7) Lee, W. H.; Kim, H. Oxidized iridium nanodendrites as catalysts for oxygen evolution reactions. *Catal. Commun.* **2011**, *12* (6), 408−411.

(8) Yu, H.; Liao, F.; Zhu, W.; Qin, K.; Shi, J.; Ma, M.; Li, Y.; Fang, M.; Su, J.; Song, B.; Li, L.; Zairov, R. R.; Ji, Y.; Shao, M.; Shao, Q. Two-Dimensional Amorphous Iridium Oxide for Acidic Oxygen Evolution Reaction. *ChemCatChem* **2023**, *15* (19), No. e202300737.

(9) Zhu, W.; Sun, Q.; Ma, M.; Liao, F.; Shao, Q.; Huang, H.; Feng, K.; Gao, D.; Chen, J.; Yang, H.; Yu, P.; Zhong, J.; Cheng, T.; Shao, M.; Liu, Y.; Kang, Z. Boosting the acidic water oxidation activity by an interfacial oxygen migration in rutile-1 T-heterophase IrO2 catalysts. *Nano Energy* **2024**, *131*, 110280.

(10) Bernsmeier, D.; Bernicke, M.; Schmack, R.; Sachse, R.; Paul, B.; Bergmann, A.; Strasser, P.; Ortel, E.; Kraehnert, R. Oxygen Evolution Catalysts Based on Ir−Ti Mixed Oxides with Templated Mesopore Structure: Impact of Ir on Activity and Conductivity. *ChemSusChem* **2018**, *11* (14), 2367−2374.

(11) Cherevko, S.; Geiger, S.; Kasian, O.; Mingers, A.; Mayrhofer, K. J. J. Oxygen evolution activity and stability of iridium in acidic media. Part 1. − Metallic iridium. *J. Electroanal. Chem.* **2016**, *773*, 69−78.
(12) Cherevko, S.; Geiger, S.; Kasian, O.; Mingers, A.; Mayrhofer, K. J. J. Oxygen evolution activity and stability of iridium in acidic media. Part 2. − Electrochemically grown hydrous iridium oxide. *J. Electroanal. Chem.* **2016**, *774*, 102−110.
(13) Lončar, A.; Escalera-López, D.; Cherevko, S.; Hodnik, N. Inter-relationships between Oxygen Evolution and Iridium Dissolution Mechanisms. *Angew. Chem., Int. Ed.* **2022**, *61* (14), No. e202114437.
(14) Ferner, K. J.; Litster, S. Composite Anode for PEM Water Electrolyzers: Lowering Iridium Loadings and Reducing Material Costs with a Conductive Additive. *ACS Appl. Energy Mater.* **2024**, *7* (18), 8124−8135.
(15) Ledendecker, M.; Geiger, S.; Hengge, K.; Lim, J.; Cherevko, S.; Mingers, A. M.; Göhl, D.; Fortunato, G. V.; Jalalpoor, D.; Schüth, F.; Scheu, C.; Mayrhofer, K. J. J. Towards maximized utilization of iridium for the acidic oxygen evolution reaction. *Nano Res.* **2019**, *12* (9), 2275−2280.
(16) Frisch, M.; Raza, M. H.; Ye, M. Y.; Sachse, R.; Paul, B.; Gunder, R.; Pinna, N.; Kraehnert, R. ALD-Coated Mesoporous Iridium-Titanium Mixed Oxides: Maximizing Iridium Utilization for an Outstanding OER Performance. *Adv. Mater. Interfaces* **2022**, *9* (6), 2102035.
(17) Böhm, D.; Beetz, M.; Gebauer, C.; Bernt, M.; Schröter, J.; Kornherr, M.; Zoller, F.; Bein, T.; Fattakhova-Rohlfing, D. Highly conductive titania supported iridium oxide nanoparticles with low overall iridium density as OER catalyst for large-scale PEM electrolysis. *Appl. Mater. Today* **2021**, *24*, 101134.
(18) van der Merwe, M.; Garcia-Diez, R.; Lahn, L.; Wibowo, R. E.; Frisch, J.; Gorgoi, M.; Yang, W.; Ueda, S.; Wilks, R. G.; Kasian, O.; Bär, M. The Chemical and Electronic Properties of Stability-Enhanced, Mixed Ir-TiOx Oxygen Evolution Reaction Catalysts. *ACS Catal.* **2023**, *13* (23), 15427−15438.
(19) Kim, M. Y.; Ban, H.-J.; Song, Y.-W.; Lim, J.; Park, S.-J.; Kim, W. J.; Hong, Y.; Kang, B.-S.; Kim, H.-S. Synthesis and electrochemical properties of nano-composite IrO2/TiO2 anode catalyst for SPE electrolysis cell. *Int. J. Hydrogen Energy* **2022**, *47* (73), 31098−31108.
(20) Bernicke, M.; Bernsmeier, D.; Paul, B.; Schmack, R.; Bergmann, A.; Strasser, P.; Ortel, E.; Kraehnert, R. Tailored mesoporous Ir/TiOx: Identification of structure-activity relationships for an efficient oxygen evolution reaction. *J. Catal.* **2019**, *376*, 209−218.
(21) Park, J.; Liu, E.; Angizi, S.; Abdellah, A.; Kirici, E. Y.; Higgins, D. Formation of Core-Shell Ir@TiO2 Nanoparticles through Hydrogen Treatment as Acidic Oxygen Evolution Reaction Catalysts. *Adv. Funct. Mater.* **2024**, *34*, 2408848.
(22) Dimitrova, N.; Banti, A.; Spyridou, O. N.; Papaderakis, A.; Georgieva, J.; Sotiropoulos, S.; Valova, E.; Armyanov, S.; Tatchev, D.; Hubin, A.; Baert, K. Photodeposited IrO2 on TiO2 support as a catalyst for oxygen evolution reaction. *J. Electroanal. Chem.* **2021**, *900*, 115720.
(23) Banti, A.; Zafeiridou, C.; Charalampakis, M.; Spyridou, O.-N.; Georgieva, J.; Binas, V.; Mitrousi, E.; Sotiropoulos, S. IrO2 Oxygen Evolution Catalysts Prepared by an Optimized Photodeposition Process on TiO2 Substrates. *Molecules* **2024**, *29* (10), 2392.
(24) Islam, J.; Yoon, B. S.; Thien, P. T.; Ko, C. H.; Kim, S.-K. Enhancing oxygen evolution reaction performance in PEM water electrolyzers through support pore structure optimization. *Catal. Today* **2024**, *425*, 114349.
(25) Wang, T.; Zeng, Y.; Xu, M.; Zhang, J.; Wu, S.; Mu, S.; Yu, J. Effect of B-Doping and Manifestation on TiO2-Supported IrO2 for Oxygen Evolution Reaction in Water Electrolysis. *Langmuir* **2023**, *39* (11), 4005−4014.
(26) Gebauer, C.; Fischer, P.; Wassner, M.; Diemant, T.; Jusys, Z.; Hüsing, N.; Behm, R. J. Performance of titanium oxynitrides in the electrocatalytic oxygen evolution reaction. *Nano Energy* **2016**, *29*, 136−148.
(27) Koderman Podboršek, G.; Suhadolnik, L.; Lončar, A.; Bele, M.; Hrnjić, A.; Marinko, Z.; Kovač, J.; Kokalj, A.; Gašparič, L.; Surca, A. K.; Kamšek, A. R.; Dražić, G.; Gaberšček, M.; Hodnik, N.; Jovanovič, P. Iridium Stabilizes Ceramic Titanium Oxynitride Support for Oxygen Evolution Reaction. *ACS Catal.* **2022**, *12* (24), 15135−15145.
(28) Suhadolnik, L.; Bele, M.; Čekada, M.; Jovanovič, P.; Maselj, N.; Lončar, A.; Dražić, G.; Šala, M.; Hodnik, N.; Kovač, J.; Montini, T.; Melchionna, M.; Fornasiero, P. Nanotubular TiOxNy-Supported Ir Single Atoms and Clusters as Thin-Film Electrocatalysts for Oxygen Evolution in Acid Media. *Chem. Mater.* **2023**, *35* (6), 2612−2623.
(29) Liu, G. Y.; Hou, F. G.; Wang, X. D.; Fang, B. Z. Robust Porous TiN Layer for Improved Oxygen Evolution Reaction Performance. *Materials* **2022**, *15* (21), 7602.
(30) Wang, S.; Lv, H.; Bi, S.; Li, T.; Sun, Y.; Ji, W.; Feng, C.; Zhang, C. Defects tailoring IrO2@TiN1+x nano-heterojunctions for superior water oxidation activity and stability. *Mater. Chem. Front.* **2021**, *5* (22), 8047−8055.
(31) Zhang, K.; Mai, W.; Li, J.; Wang, H.; Li, G.; Hu, W. Highly scattered Ir oxides on TiN as an efficient oxygen evolution reaction electrocatalyst in acidic media. *J. Mater. Sci.* **2020**, *55* (8), 3507−3520.
(32) Karade, S. S.; Sharma, R.; Hedegaard, M. A. B.; Andersen, S. M. Stepwise Understanding on Hydrolysis Formation of the IrOx Nanoparticles as Highly Active Electrocatalyst for Oxygen Evolution Reaction. *Electrocatalysis* **2024**, *15* (4), 291−300.
(33) Sadeghi, E.; Morgen, P.; Makovec, D.; Gyergyek, S.; Sharma, R.; Andersen, S. M. Scalable Solid-State Synthesis of Carbon-Supported Ir Electrocatalysts for Acidic Oxygen Evolution Reaction: Exploring the Structure−Activity Relationship. *ACS Appl. Mater. Interfaces* **2024**, *16* (40), 53750−53763.
(34) Kim, E. J.; Kim, K. h.; Bak, J.; Lee, K.; Cho, E. Carbon nanotube−titanium dioxide nanocomposite support for improved activity and stability of an iridium catalyst toward the oxygen evolution reaction. *RSC Adv.* **2022**, *12* (55), 35943−35949.
(35) Chen, Q.; Li, J.; Chen, Q.; Ostrikov, K. Recent advances towards aqueous hydrogen peroxide formation in a direct current plasma−liquid system. *High Voltage* **2022**, *7* (3), 405−419.
(36) Rezaei, F.; Vanraes, P.; Nikiforov, A.; Morent, R.; De Geyter, N. Applications of Plasma-Liquid Systems: A Review. *Materials* **2019**, *12* (17), 2751.
(37) Chen, Q.; Li, J.; Li, Y. A review of plasma−liquid interactions for nanomaterial synthesis. *J. Phys. D: Appl. Phys.* **2015**, *48* (42), 424005.
(38) Treshchalov, A.; Erikson, H.; Puust, L.; Tsarenko, S.; Saar, R.; Vanetsev, A.; Tammeveski, K.; Sildos, I. Stabilizer-free silver nanoparticles as efficient catalysts for electrochemical reduction of oxygen. *J. Colloid Interface Sci.* **2017**, *491*, 358−366.
(39) Hussain, S.; Erikson, H.; Kongi, N.; Treshchalov, A.; Rähn, M.; Kook, M.; Merisalu, M.; Matisen, L.; Sammelselg, V.; Tammeveski, K. Oxygen Electroreduction on Pt Nanoparticles Deposited on Reduced Graphene Oxide and N-doped Reduced Graphene Oxide Prepared by Plasma-assisted Synthesis in Aqueous Solution. *ChemElectroChem* **2018**, *5* (19), 2902−2911.
(40) Lüsi, M.; Erikson, H.; Treshchalov, A.; Rähn, M.; Merisalu, M.; Kikas, A.; Kisand, V.; Sammelselg, V.; Tammeveski, K. Oxygen reduction reaction on Pd nanocatalysts prepared by plasma-assisted synthesis on different carbon nanomaterials. *Nanotechnology* **2021**, *32* (3), 035401.
(41) Hussain, S.; Kongi, N.; Treshchalov, A.; Kahro, T.; Rähn, M.; Merisalu, M.; Tamm, A.; Sammelselg, V.; Tammeveski, K. Enhanced oxygen reduction reaction activity and durability of Pt nanoparticles deposited on graphene-coated alumina nanofibres. *Nanoscale Adv.* **2021**, *3* (8), 2261−2268.
(42) Hujjatul Islam, M.; Paul, M. T. Y.; Burheim, O. S.; Pollet, B. G. Recent developments in the sonoelectrochemical synthesis of nanomaterials. *Ultrason. Sonochem.* **2019**, *59*, 104711.
(43) Ye, Y.; Pui, D. Y. H. Detection of nanoparticles suspended in a light scattering medium. *Sci. Rep.* **2021**, *11* (1), 20268.
(44) Moriau, L.; Nazrulla, M. A.; Logar, A.; Pavko, L.; Bele, M.; Hodnik, N.; Surca, A. K. Ir metal nanoparticles and IrO2 for acidic

https://doi.org/10.1021/acsaem.5c00444
ACS Appl. Energy Mater. 2025, 8, 7084−7094

oxygen evolution reaction: Insight from Raman spectroscopy. *Sustain. Mater. Technol.* **2024**, *40*, No. e00901.
(45) Bele, M.; Jovanovič, P.; Marinko, Z.; Drev, S.; Šelih, V. S.; Kovač, J.; Gaberščček, M.; Koderman Podboršek, G.; Dražić, G.; Hodnik, N.; Kokalj, A.; Suhadolnik, L. Increasing the Oxygen-Evolution Reaction Performance of Nanotubular Titanium Oxynitride-Supported Ir Nanoparticles by a Strong Metal−Support Interaction. *ACS Catal.* **2020**, *10* (22), 13688−13700.
(46) Choi, M.-J.; Park, H.; Engelhard, M. H.; Li, D.; Sushko, P. V.; Du, Y. Reevaluation of XPS Pt 4f peak fitting: Ti 3s plasmon peak interference and Pt metallic peak asymmetry in Pt@TiO2 system. *J. Vac. Sci. Technol., A* **2024**, *42* (6), 063209.
(47) Greczynski, G.; Jensen, J.; Greene, J. E.; Petrov, I.; Hultman, L. X-ray Photoelectron Spectroscopy Analyses of the Electronic Structure of Polycrystalline Ti1-xAlxN Thin Films with $0 \leq x \leq 0.96$. *Surf. Sci. Spectra* **2014**, *21* (1), 35−49.
(48) Pauporté, T.; Andolfatto, F.; Durand, R. Some electrocatalytic properties of anodic iridium oxide nanoparticles in acidic solution. *Electrochim. Acta* **1999**, *45* (3), 431−439.
(49) Zhang, K.; Guo, C.; Wu, Y.; Yao, R.; Zhao, Q.; Li, J.; Liu, G. Amorphous iridium oxide coating on TiO2 for efficient electrocatalytic oxygen evolution reaction. *Int. J. Hydrogen Energy* **2024**, *69*, 1105−1112.
(50) Ohno, H.; Nohara, S.; Kakinuma, K.; Uchida, M.; Miyake, A.; Deki, S.; Uchida, H. Remarkable Mass Activities for the Oxygen Evolution Reaction at Iridium Oxide Nanocatalysts Dispersed on Tin Oxides for Polymer Electrolyte Membrane Water Electrolysis. *J. Electrochem. Soc.* **2017**, *164* (9), F944.
(51) Moriau, L.; Koderman Podboršek, G.; Surca, A. K.; Semsari Parpari, S.; Šala, M.; Petek, U.; Bele, M.; Jovanovič, P.; Genorio, B.; Hodnik, N. Enhancing Iridium Nanoparticles' Oxygen Evolution Reaction Activity and Stability by Adjusting the Coverage of Titanium Oxynitride Flakes on Reduced Graphene Oxide Nanoribbons' Support. *Adv. Mater. Interfaces* **2021**, *8* (17), 2100900.
(52) Hartig-Weiss, A.; Tovini, M. F.; Gasteiger, H. A.; El-Sayed, H. A. OER Catalyst Durability Tests Using the Rotating Disk Electrode Technique: The Reason Why This Leads to Erroneous Conclusions. *ACS Appl. Energy Mater.* **2020**, *3* (11), 10323−10327.
(53) Geiger, S.; Kasian, O.; Mingers, A. M.; Nicley, S. S.; Haenen, K.; Mayrhofer, K. J. J.; Cherevko, S. Catalyst Stability Benchmarking for the Oxygen Evolution Reaction: The Importance of Backing Electrode Material and Dissolution in Accelerated Aging Studies. *ChemSusChem* **2017**, *10* (21), 4140−4143.

https://doi.org/10.1021/acsaem.5c00444
ACS Appl. Energy Mater. 2025, 8, 7084−7094